The Deepening of Tropical Convection by Congestus Preconditioning

MICHAEL L. WAITE* AND BOUALEM KHOUIDER

Department of Mathematics and Statistics, University of Victoria, Victoria, British Columbia, Canada

(Manuscript received 19 October 2009, in final form 2 February 2010)

ABSTRACT

The role of environmental moisture in the deepening of cumulus convection is investigated by means of cloud-resolving numerical experiments. Under idealized conditions of uniform SST and specified radiative cooling, the evolution of trade wind cumulus into congestus clouds, and ultimately deep convection, is simulated and analyzed. The results exhibit a tight coupling between environmental moisture and cloud depth, both of which increase over the course of the simulations. Moistening in the lower troposphere is shown to result from the detrainment of water vapor from congestus clouds, and the strength of this tendency is quantified. Moistening of the lower troposphere reduces the dilution of cloud buoyancy by dry-air entrainment, and the relationship between this effect and increasing cloud depth is examined. The authors confirm that the mixing of water vapor by subgrid-scale turbulence has a significant impact on cloud depth, while the mixing of sensible heat has a negligible effect. By contrast, the dependence of cloud depth on CAPE appears to be of secondary importance. However, the deepening trend observed in these simulations is not solely determined by the evolving mean vapor profile. While enhancing the horizontally averaged humidity does result in deeper clouds, this occurs only after an adjustment period of several hours, presumably because of the buildup of CAPE. The implications of these findings for large-scale simulations in which resolved mixing is reduced—for example, by coarser spatial resolution or 2D experiments—are also discussed.

1. Introduction

Cumulus convection in the tropics is dominated by three principal cloud types: shallow cumulus, which detrain at the boundary layer inversion; cumulus congestus, which extend into the midtroposphere; and deep cumulonimbus, which reach the upper troposphere (e.g., Johnson et al. 1999; Takayabu et al. 2010). While the fundamental role of shallow and deep cumulus has been long recognized, the distinct importance of congestus has become apparent only more recently (Johnson et al. 1999). These clouds are frequently associated with low humidity in the midtroposphere, where the turbulent entrainment of dry air is thought to dilute cloud buoyancy and inhibit the development of deep cumulonimbus, even in the presence of significant CAPE (e.g., Brown and Zhang 1997; Zhang and Chou 1999; Takemi et al. 2004). At the same time, congestus clouds feed back on the vapor field of the midtroposphere by moistening through detrainment, horizontal convergence from low-level heating, and the associated precipitation drying (e.g., Nitta and Esbensen 1974; Takayabu et al. 2010). As a result, they possess the potential to transform or ''precondition'' their environment into one that may be more favorable for deep convection (e.g., Johnson et al. 1999). This two-way relationship between congestus clouds and tropospheric moisture, in which congestus clouds potentially moisten their surroundings, while enhanced moisture promotes deeper convection, is the focus of this paper. This relationship is not a new idea; it has been widely recognized and demonstrated qualitatively in both observations and numerical simulations (Brown and Zhang 1997; Johnson et al. 1999; Straub and Kiladis 2002; Takemi et al. 2004; Derbyshire et al. 2004; Kiladis et al. 2005; Kuang and Bretherton 2006; Kiladis et al. 2009; Holloway and Neelin 2009; Zhang and Hagos 2009; Takayabu et al. 2010). But the question of how it occurs and operates remains open. Our main goal here is to identify, assess, and quantify the various physical mechanisms that are believed to be responsible for this effect, such as turbulent mixing,

* Current affiliation: Department of Applied Mathematics, University of Waterloo, Waterloo, Ontario, Canada.

Corresponding author address: Michael L. Waite, Department of Applied Mathematics, University of Waterloo, Waterloo ON N2L 3G1, Canada.
E-mail: mwaite@uwaterloo.ca

DOI: 10.1175/2010JAS3357.1

background moisture, and CAPE. Furthermore, we aim to quantify these processes for use in stochastic model parameterizations of organized tropical convection (Khouider et al. 2010).

Preconditioning and the associated transitions from shallow to deep convective regimes are believed to play a key role in tropical meteorology, particularly for the dynamics of convectively coupled equatorial waves, and have important implications for theory and parameterization [for a review, see Kiladis et al. (2009)]. Shallow cumulus are observed to grow into congestus in advance of deep cumulonimbus towers in a variety of dynamical structures on different scales, including convectively coupled Kelvin waves (Straub and Kiladis 2002), inertia–gravity waves (Haertl and Kiladis 2004), and the MJO (Kiladis et al. 2005). Deep convection is then followed by stratiform clouds, which generate evaporation-driven downdrafts that dry the boundary layer and contribute to the suppression of deep convection (e.g., Kiladis et al. 2009). The ubiquity of this backward vertical tilt, with shallower clouds preceding deeper clouds, has been attributed in part to moistening of the lower troposphere by congestus clouds (e.g., Kiladis et al. 2009); preconditioning thereby influences the basic characteristics of observed convectively coupled waves and has consequently been incorporated into idealized models for these waves (Khouider and Majda 2006, 2008; Waite and Khouider 2009; Khouider et al. 2010). These effects have proven challenging to parameterize in large-scale models; indeed, the insensitivity of cloud mass flux to tropospheric humidity in some convective parameterizations, and the resulting lack of shallow and congestus clouds in dry environments, has been linked with poor simulations of convectively coupled waves and the MJO (Lin et al. 2006; Zhang and Hagos 2009).

Cloud-resolving model (CRM) simulations are a useful tool for exploring the connection between tropospheric humidity and cumulus cloud height. Takemi et al. (2004) found deep convection to be inhibited in the presence of dry layers in the middle and upper troposphere in tropical western Pacific sounding data. They confirmed this relationship in 2D CRM simulations, in which only shallow cumulus developed when mean humidity profiles were maintained at relatively dry levels. Furthermore, they showed that increasing the moisture content of the lower troposphere in the imposed sounding to values representative of strongly disturbed conditions yielded congestus and deep cumulus clouds when the moist layer extended above 4 km. By contrast, the effect of reducing the dry lapse rate of the midlevel stable layer by 35% in their simulations was much weaker. In a similar study, Derbyshire et al. (2004) used 3D CRM simulations to investigate the convective regimes associated with different imposed humidity soundings. They found a clear relationship between free-tropospheric moisture and the depth of cumulus convection. Relative humidity values of 25% in the free troposphere (FT) yielded mainly shallow convection, values of 90% led to deep convection, and intermediate values facilitated the development of deeper clouds with increased moisture. The physical mechanism for the impact of tropospheric moisture on cloud depth has been attributed to the entrainment of dry environmental air: cumulus clouds in relatively dry surroundings experience more dry-air entrainment, and consequently less net condensation, latent heating, and buoyancy, than clouds in moister environments (e.g., Brown and Zhang 1997; Holloway and Neelin 2009).

The computational studies referenced above considered quasi-stationary convection resulting from an imposed moisture profile, which is not allowed to evolve via moistening by the clouds themselves. As a result, these simulations do not directly elucidate the transient problem of convective cloud deepening. This question was considered by Kuang and Bretherton (2006), who simulated a transition from shallow to congestus and eventually to deep convection in a 3D CRM. The increase in cloud depth was initiated by artificially increasing the surface fluxes of sensible and latent heat in the trade wind cumulus test case of Siebesma et al. (2003), in which shallow convection is sustained by surface fluxes, radiative cooling, and large-scale forcing. After the increase, congestus clouds appear, and after several days they deepen into cumulonimbus. By restarting their simulation in the congestus phase with enhanced free-tropospheric moisture, Kuang and Bretherton (2006) were able to accelerate the transition to deep convection. Though extremely suggestive, these results raise a number of questions that were not directly addressed by Kuang and Bretherton (2006): What are the mechanisms by which congestus clouds moisten their environment? How dependent is the simulated transition from shallow to deep convection on resolved and subgrid-scale mixing? What is the relative importance of free-tropospheric moistening and the buildup of CAPE through radiative cooling and boundary layer moistening? In this work, we address these questions with 3D CRM simulations that investigate the two-way relationship between cloud-induced moistening and the deepening of cumulus convection. Our setup is somewhat similar to that of Kuang and Bretherton (2006), but our strategy for inducing a transition from shallow to deep convection is different: rather than increasing the surface fluxes, we omit the large-scale forcing terms that were necessary to sustain shallow convection and keep the troposphere dry in Siebesma et al. (2003). We thus

allow a more natural moistening of the free troposphere and ultimate transition to deep convection. A number of new sensitivity experiments and diagnostics are presented to address the questions outlined above.

The numerical model and approach are described in the next section, and results and analysis are presented in section 3. An overview of the control simulation is given in section 3a, in which a clear connection is apparent between tropospheric moisture and cloud depth, with the deep convective regime having a much moister environment than the shallow cumulus and congestus phases at earlier times. This moistening is a result of congestus clouds, and in section 3b we quantify its magnitude and identify the physical mechanisms responsible. The sensitivity of our results to subgrid-scale and resolved mixing is investigated in section 3c. In section 3d, we present experiments that diagnose the importance of free-tropospheric moistening and cooling on the transition to deep convection, and the separate dependence on boundary layer moistening is considered in section 3e. Conclusions are given in section 4.

2. Methodology

a. Numerical model

Simulations were performed with the Eulerian/semi-Lagrangian model EULAG, which integrates the 3D nonhydrostatic anelastic equations of motion with a second-order accurate, semi-implicit, flux-form Eulerian, non-oscillatory forward-in-time approach (see Smolarkiewicz and Margolin 1998; Smolarkiewicz and Prusa 2005; Grabowski and Smolarkiewicz 2002, and references therein). There are seven prognostic variables: the three components of velocity $\mathbf{u} = (u, v, w)$, potential temperature θ, and mixing ratios of water vapor q_v, cloud condensate q_c, and precipitation condensate q_p. We use the microphysics parameterization of Grabowski (1998), which assumes, for the purposes of determining saturation pressure, precipitation growth, and terminal velocities, that the condensate is liquid water for temperatures above 0°C, ice for temperatures below −10°C, and a linear mixture for intermediate values. Condensation rates in the model are computed following Grabowski and Smolarkiewicz (1990).

The computational domain has dimensions of 20 km in the horizontal and vertical. Boundary conditions are periodic in x and y and free slip in z, with a gravity wave–absorbing layer in the upper 4 km of the domain. The grid spacing is uniformly 100 m in the horizontal and vertical directions, and the time step is 2.5 s. Our domain size and grid spacing are chosen to be intermediate between small-scale high-resolution large-eddy simulation (LES) of shallow cumulus [with $\Delta x = O(10)$ m; e.g., Zhao and Austin 2005] and large-scale CRM simulations of deep convective organization [with $\Delta x = O(1)$ km, e.g., Tulich et al. 2007]. The effects of subgrid-scale turbulent mixing on momentum and scalars are represented with a Smagorinsky–Lilly closure (Lilly 1962; Smagorinsky 1963), assuming a Prandtl number of 0.42. Coriolis terms and topography are neglected.

b. Initial conditions

The initial profiles of potential temperature, water vapor, and relative humidity are plotted in Fig. 1. These profiles are chosen to favor the development of shallow cumulus clouds during the early stage of the simulation. In the boundary layer we use the idealized Barbados Oceanographic and Meteorological Experiment (BOMEX) soundings of Siebesma et al. (2003), which are representative of a shallow trade wind cumulus regime with no congestus or deep convection. These profiles are characterized by a strong boundary layer inversion and dry lower troposphere, with relative humidity above the inversion of less than 30%. We extend the soundings in the vertical by assuming a vapor scale height of 2 km and a uniform dry Brunt–Väisälä frequency of 0.01 s^{-1} in the free troposphere and 0.02 s^{-1} in the stratosphere, with the tropopause at 15 km. These piecewise linear profiles are smoothed in the vertical to avoid discontinuities in stability. Kuang and Bretherton (2006) used the same boundary layer profiles but extended them differently by including a layer of weak static stability in the upper troposphere to enhance the development of deep convection (see their Fig. 2). An initial uniform zonal velocity of 10 m s^{-1} is included to drive the surface fluxes (described below). Random perturbations in potential temperature, with uniformly distributed values between ±0.1 K, are added to the mixed layer to break the horizontal symmetry in the initial conditions and forcing.

c. Forcing

Convection is initiated and sustained by surface fluxes and radiative cooling. Surface fluxes of sensible heat and moisture are computed following the idealized approach of Grabowski (1998), and momentum fluxes are computed similarly. The sea surface temperature is assumed to be 300.4 K, which is consistent with the initial soundings (Siebesma et al. 2003). The radiative cooling rate is prescribed to be 2 K day^{-1} in the boundary layer ($z \leq$ 1.5 km), decreasing linearly to 1 K day^{-1} in the free troposphere ($3 \leq z \leq 12$ km) and decreasing to zero in the stratosphere ($z \geq 15$ km) (also following Siebesma et al. 2003). The mean wind of 10 m s^{-1} is maintained by

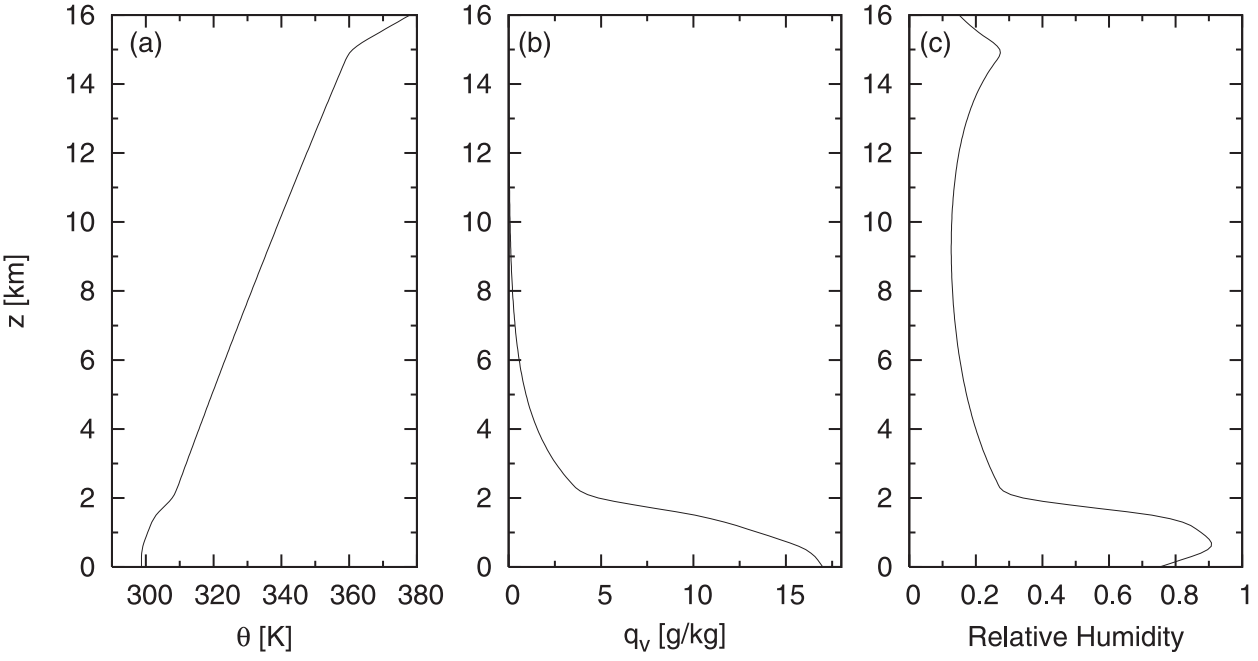

FIG. 1. Initial profiles of (a) θ, (b) q_v, and (c) relative humidity.

relaxing the horizontally averaged velocity with a time scale of 12 h; no relaxation is applied to the thermodynamic fields.

To allow for a natural transition from shallow to deeper convection, we have not included the large-scale subsidence, advection, pressure gradient, and low-level drying forcing terms of Siebesma et al. (2003). These forcings were carefully specified to balance the surface fluxes and radiative cooling in their simulation, and yield a statistically stationary shallow cumulus regime after a spinup period of a few hours. By contrast, our forcings are chosen to be out of equilibrium in order to simulate the deepening of shallow cumulus into congestus clouds. By omitting these forcing terms, particularly drying by prescribed large-scale subsidence, we allow the shallow cumulus clouds to modify their environment and possibly transition to a deeper convective regime. Our approach is different from that of Kuang and Bretherton (2006), who included most of the large-scale forcings of Siebesma et al. (2003) and initiated a transition by doubling the strength of the surface fluxes. We do include the mixed-layer drying term of Siebesma et al. (2003) in one simulation (see section 3e) to examine the effect of limiting boundary layer moisture and CAPE. The control simulation is integrated for 48 h. Various sensitivity experiments were also performed to examine the dependence of these results on moisture and mixing. Simulations are summarized in Table 1 and described in detail below.

3. Results

a. Overview of simulation

After an initial spinup, the simulation evolves through three phases, which are visible in the time series of vertical profiles $\overline{q}_l \equiv \overline{q}_c + \overline{q}_p$, where the overbar denotes the horizontal domain average (Fig. 2a): shallow cumulus ($6 \lesssim t \lesssim 20$ h), transition congestus ($20 \lesssim t \lesssim 32$ h), and deep convection ($t \gtrsim 32$ h). The domain average is employed for simplicity, but our tests show that it closely approximates the environmental average restricted to cloud-free grid cells. Time series of $\overline{q}'_v$ and $\overline{\theta}'$, where

TABLE 1. Summary of simulations. Start times greater than 0 h imply restart from control run.

Run	Time (h)	Description
1	0–48	Control simulation
2	20–32	No subgrid-scale mixing of q_v in FT
3	20–32	No subgrid-scale mixing of θ in FT
4	0–48	Low resolution: $\Delta x = \Delta y = 500$ m
5	0–48	2D: $v = 0$, $\partial/\partial y = 0$
6	20–32	Moist restart: FT q_v sounding at $t = 20$ h from $t = 32$ h
7	20–32	Moist restart: FT q_v sounding at $t = 20$ h from $t = 48$ h
8	20–32	Cool restart: FT θ sounding at $t = 20$ h from $t = 32$ h
9	20–32	Cool restart: FT θ sounding at $t = 20$ h from $t = 48$ h
10	0–60	Mixed layer drying

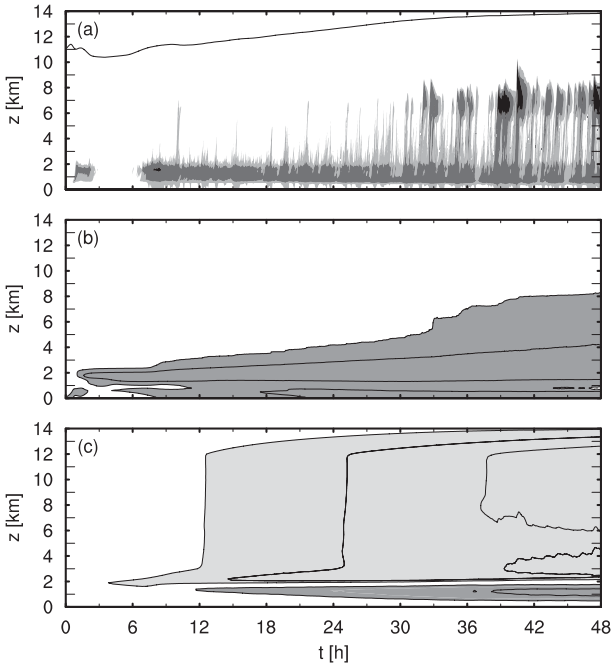

FIG. 2. Time series of horizontally averaged profiles of (a) q_l, (b) q_v', and (c) θ'. In (a), $\overline{q}_l$ values over 10^{-4} g kg^{-1} are light gray, values over 10^{-3} g kg^{-1} are dark gray, values over 10^{-2} g kg^{-1} are black, and the LNB is also shown (solid line). In (b), contours are drawn at 0.1 and 1 g kg^{-1}, and $\overline{q}_v'$ values over 0.1 g kg^{-1} are shaded. In (c), contours are drawn every ± 0.5 K, and $\overline{\theta}'$ values over 0.5 K and under -0.5 K are shaded dark and light gray, respectively.

prime denotes fluctuations from the initial conditions, are also shown in Fig. 2. The spinup phase ($t \lesssim 6$ h) is characterized by an initial burst of shallow convection, followed by a cloud-free period of several hours during which CAPE and boundary layer moisture are restored by surface fluxes (see Fig. 5). Quasi-stationary shallow cumulus develop around $t = 6$ h and persist until $t \approx 20$ h. Cloud tops during this period lie primarily between 2 and 3 km, with an occasional anomalously buoyant clouds reaching higher levels (see, e.g., Fig. 2a around $t = 10$ h). These sporadic deep clouds were not obtained by Siebesma et al. (2003) because they are suppressed by imposed large-scale subsidence. However, cloud tops exceeding 4 km occur only a handful of times before $t = 20$ h.

After $t \approx 20$ h, the frequency with which clouds reach the midtroposphere increases, although the deepest clouds continue to be quite intermittent. The free troposphere moistens at low levels and cools during this phase (Figs. 2b,c). The congestus clouds of the transition phase are relatively short lived, with time scales $O(10)$ min. The deepening trend continues until around $t = 32$ h, after which deep, larger-scale clouds develop, with heights of more than 8 km and time scales $O(1)$ h. We refer to these clouds as deep convection, but unlike the deep cumulonimbus obtained by Kuang and Bretherton (2006), they do not penetrate to the tropopause. This discrepancy is a result of the static stability of the upper troposphere in our initial soundings, which is stronger than the near-neutral stability prescribed at these levels by Kuang and Bretherton (2006). Nevertheless, the evolving vertical extent of the congestus clouds in the transition period of our simulation presents a useful idealized framework for studying the effects of tropospheric moisture and preconditioning on the deepening of convection. The level of neutral buoyancy (LNB), computed by reversibly lifting a horizontally averaged mixed layer parcel through the mean sounding at a given time, is also shown in Fig. 2a. As in previous studies, it exceeds the observed cloud tops at all times: by a factor of 5 in the shallow cumulus regime, decreasing to a factor of 2 in the deep convection regime. The substantial difference between the observed cloud tops and LNB underlines the importance of entrainment in setting the detrainment levels of these clouds.

The evolution of an individual congestus cloud during the transition phase is illustrated in Fig. 3, which shows vertical (x–z) slices of q_v and q_l at 6-min intervals throughout the cloud life cycle. The cloud appears at $t \approx 21.5$ h, reaches a maximum height of around 7 km, and lasts for approximately 20 min. This time scale is representative of other congestus clouds in this simulation. The horizontal scale of the cloud is $O(1)$ km, which corresponds to $O(10)$ grid points. Despite our relatively high spatial resolution compared to other CRM simulations, turbulent cloud entrainment is only marginally resolved and subgrid-scale fluxes are expected to contribute significantly to the mixing of cloudy and environmental air. The cloud detrains before $t = 22$ h (Fig. 3d) and can be seen to deposit a positive moisture anomaly of several grams per kilogram in the lower free troposphere.

Profiles of potential temperature, vapor and liquid water mixing ratios, and relative humidity are shown in Fig. 4, averaged in the horizontal over the domain and in time over the three regimes identified above. Note that profiles of θ and q_v, along with their fluctuations from the initial conditions θ' and q_v', are plotted. The shallow cumulus cloud layer warms slightly as the simulation progresses, resulting in a reduced boundary layer inversion after the development of congestus clouds. The free troposphere cools by approximately 1°C during the transition from shallow to deep convection and is ultimately offset by deep-convective warming at later times. However, we will show below that this radiative cooling alone is not sufficient to trigger deep convection when the environment is dry (see section 3d). There is no significant warming in the mixed layer, implying that the

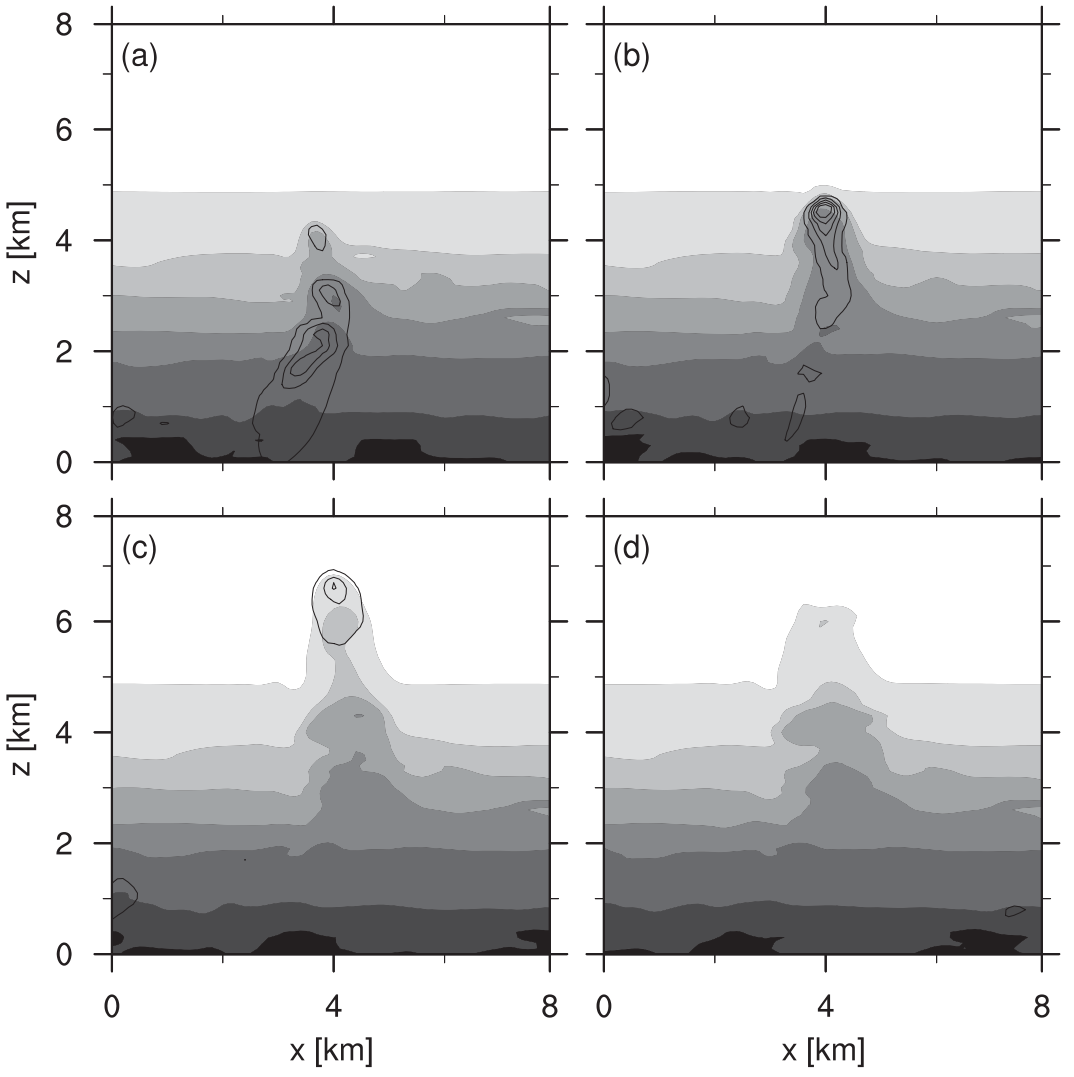

FIG. 3. Vertical (x–z) slice of q_v (shaded) and q_l (solid lines), in the control run for $t = 21$ h + (a) 32, (b) 38, (c) 44, and (d) 50 min. Only a subset of the domain, translated to stay centered on the cloud, is shown, and fields are averaged in y over 1 km. Vapor contours are drawn at 1, 2, 3, 5, 10, 15, and 18 g kg^{-1}, and q_l contours are drawn at 0.025, 0.25, 0.5, 0.75, and 1 g kg^{-1}.

surface fluxes and radiative cooling are in approximate equilibrium with the mixed layer dynamics.

Moistening $O(1)$ g kg^{-1} is observed over two distinct layers: in the mixed layer ($z \lesssim 500$ m) and in the lower free troposphere ($2 \lesssim z \lesssim 5$ km). This moistening is also evident in Fig. 5a, which shows time series of q_v averaged over these two layers. The evolution of mixed layer q_v closely resembles that of CAPE (Fig. 5b), growing rapidly during the shallow cumulus and transition phases and more slowly at later times. The free tropospheric water vapor increases at all times after the development of shallow cumulus, with a growth rate that increases in the deep convection phase of the simulation. The mixed layer moistening corresponds to only a small increase in relative humidity (Fig. 4e), but the moistening in the free troposphere increases the relative humidity by $O(10)\%$. In the transition phase, the enhanced humidity is restricted to $z \lesssim 4$ km, where relative humidity increases from approximately 25%–35%. In the deep convection phase the moist layer extends up to $z \approx 6$ km. The liquid water profile of the shallow cumulus clouds is similar in the transition and deep regimes. At higher levels there is a significant increase in q_l in the last phase, corresponding to deep clouds with tops near 8 km.

b. *Moistening by congestus clouds*

The tropospheric moistening that occurs during the transition phase is clearly associated with the congestus

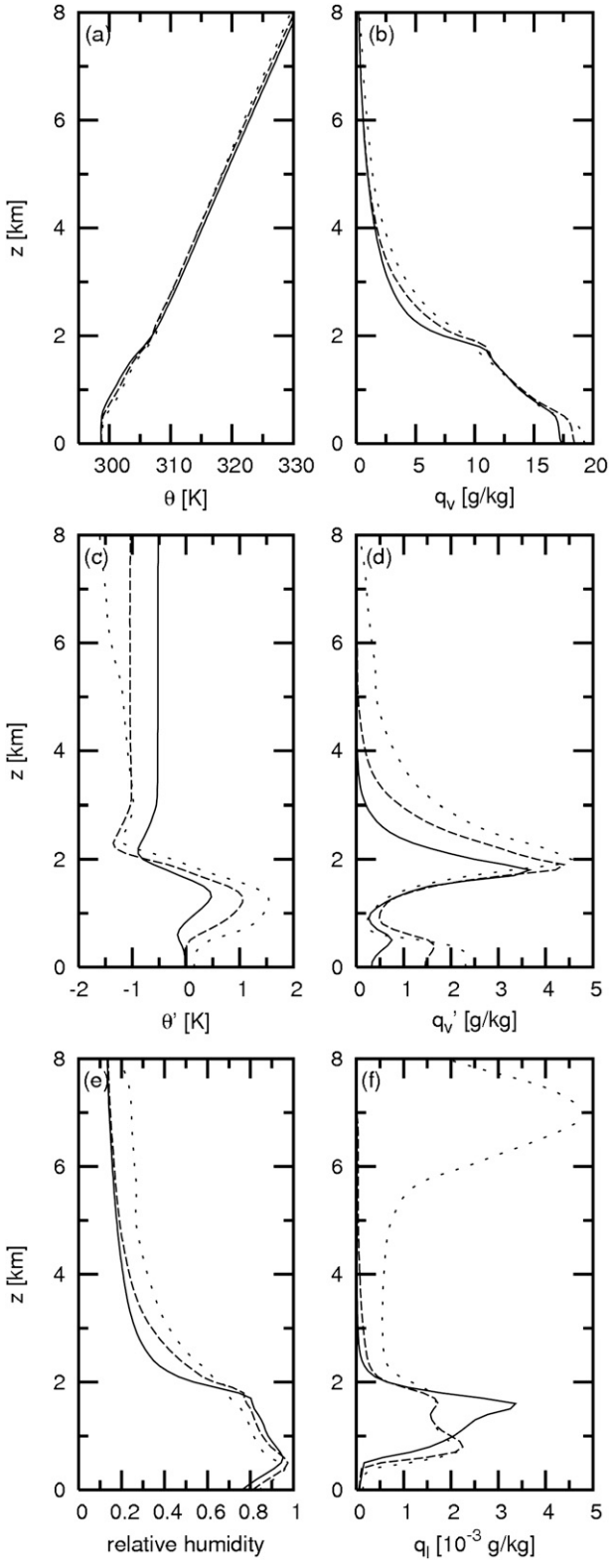

FIG. 4. Horizontally averaged profiles of (a) θ; (b) q_v; (c) θ', (d) q_v', (e) relative humidity, and (f) q_l. Profiles are averaged in time over the shallow cumulus (solid), transition (dashed), and deep (dotted) phases of the control run. The relative humidity is computed from profiles of θ and q_v.

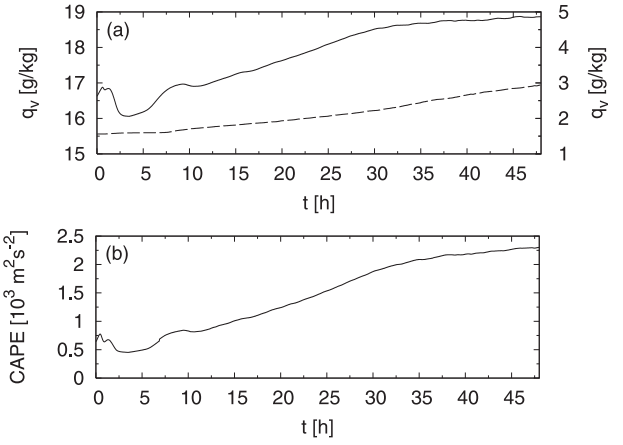

FIG. 5. (a) Time series of q_v in the control run, averaged in the horizontal over the domain and in the vertical over the mixed layer $0 \le z \le 500$ m (solid; left y axis) and lower free troposphere $2 \le z \le 5$ km (dashed; right y axis). (b) Time series of CAPE in the control run. CAPE is computed by reversibly lifting a mean mixed layer parcel through a horizontally averaged sounding at every time.

clouds of this period, since the vapor anomaly extends to higher levels as the clouds deepen. Outside the mixed layer, the evolution of $\overline{q}_v$ is determined by three terms in the horizontally averaged q_v equation: the convergence of vertical advective vapor flux, the convergence of subgrid-scale vapor flux, and net evaporation, which includes diffusion of vapor onto precipitation and evaporation of precipitation. Together, these tendencies correspond to the Q_2 budget of Yanai et al. (1973). Vertical profiles of these terms are plotted in Fig. 6 for the beginning, middle, and end of the transition period. At all times, the evolution of $\overline{q}_v$ in the free troposphere is dominated by the advective flux divergence, which includes both detrainment of vapor from clouds and subsidence between clouds. The net moistening by advection in the lower free troposphere suggests that detrainment dominates the advective tendency. Contributions from subgrid-scale fluxes and evaporation/condensation are an order of magnitude smaller at these levels, although they are more significant in the boundary layer (not shown). The detrainment of water vapor yields a maximum moistening of approximately 2 g kg^{-1} day^{-1} in the levels directly above the boundary layer throughout the transition phase, while the vertical extent of the moistening increases in time, in agreement with the vapor profiles in Fig. 4. By the end of the transition phase, moistening tendencies of more than 1 g kg^{-1} day^{-1} extend to a height of 4 km.

c. *Sensitivity to mixing*

The identification of turbulent entrainment as a key factor in setting the vertical scale of congestus clouds

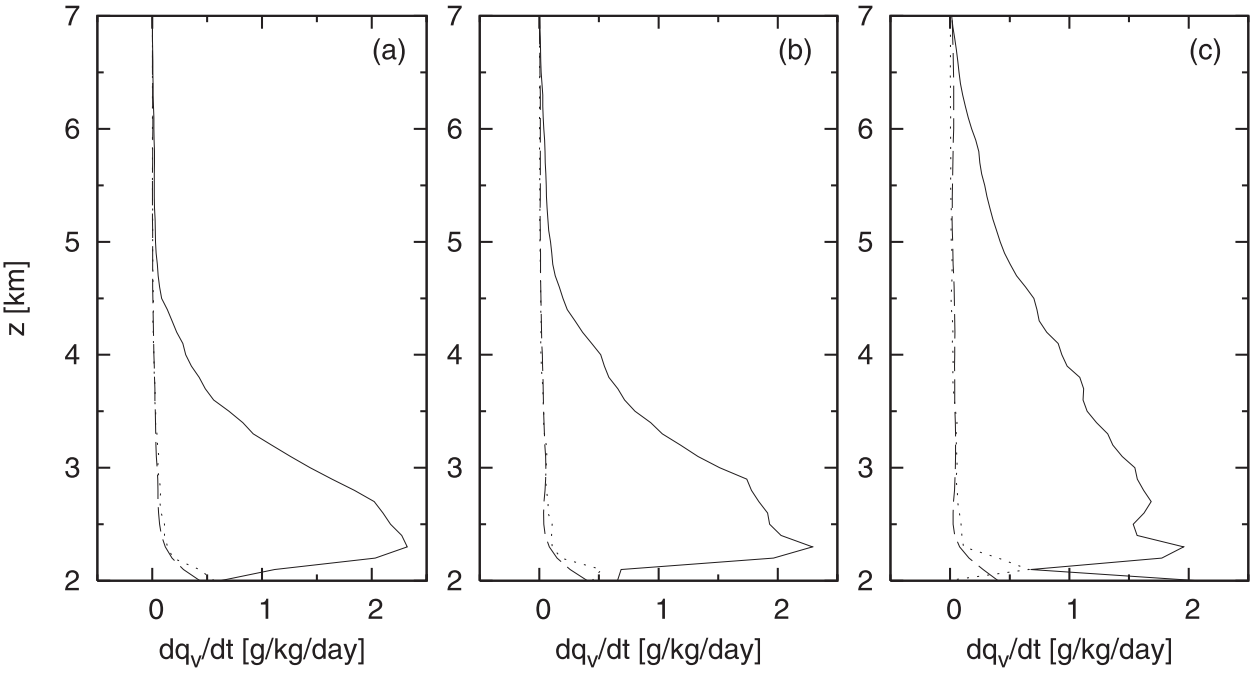

FIG. 6. Horizontal average profiles of vapor tendency in the control run due to vertical advective flux convergence (solid), net evaporation (dashed), and subgrid-scale mixing (dotted), averaged in time over (a) the early transition period $20 \le t \le 24$ h, (b) the mid-transition period $24 \le t \le 28$ h, and (c) the late transition period $28 \le t \le 32$ h. Profiles are restricted to $z \ge 2$ km to focus on the moistening of the lower free troposphere; all tendencies are larger in the boundary layer.

suggests that CRM simulations of these clouds may be sensitive to computational parameters affecting mixing. To investigate the role of subgrid-scale terms, we have performed two additional simulations in which the parameterized fluxes of θ and q_v, respectively, were omitted for $z \ge 2$ km. These simulations were started at $t =$ 20 h in the control run and integrated for 12 h to evaluate the effect of reduced mixing on the transition from shallow to deep convection. Time series of $\overline{q}_l$ are shown in Fig. 7. Omitting subgrid-scale fluxes of q_v has a noticeable effect on the simulation evolution (Fig. 7b): vigorous deep convection appears by $t = 24$ h, only a few hours after the start of the sensitivity test and significantly earlier than in the control run. By contrast, neglecting the mixing of θ has no significant impact on the transition to deep convection. Figure 8 shows domain- and cloud-averaged profiles of equivalent potential temperature θ_e for the control run and reduced mixing experiments (cloud averages are restricted to grid cells with $q_l > 0.01$ g kg^{-1}). Differences in the dependence of cloud θ_e on height reflect changes in entrainment in the simulation. It is apparent that clouds in the experiment without q_v mixing have greater values of θ_e, and consequently experience less entrainment and dilution, than clouds with q_v mixing. The simulation without subgrid-scale fluxes of θ is indistinguishable from the control run.

The importance of parameterized mixing in determining cloud evolution suggests that the transition to deep convection may be sensitive to grid resolution and the horizontal dimensionality of the simulation, which both directly impact resolved turbulence. To examine the significance of this relationship, we have rerun the control simulation for two sensitivity tests, one with a coarse horizontal grid spacing of $\Delta x = 500$ m and the other with no y dimension. Grid spacings of 500 m or more and 2D simulations are still commonly employed in CRM studies, especially for large domains [e.g., Takemi et al. (2004) and Tulich et al. (2007) performed 2D simulations with $\Delta x = 1$ and 2 km, respectively, while the simulations in Derbyshire et al. (2004) were 3D with $\Delta x = 500$ m]. The resulting time series of $\overline{q}_l$ are shown in Fig. 9. The effects of these changes in configuration are visible in both simulations, in which there is a much shorter shallow cumulus phase and an accelerated development of deep clouds relative to the control run. Deep clouds exceeding 8 km in height appear by $t =$ 22 h in both sensitivity tests, at least 10 h earlier than in the control run. Interestingly, there is essentially no transition period with congestus clouds of gradually increasing cloud depths, but rather an abrupt jump from shallow to deep convection.

The time series of CAPE from both experiments are shown in Fig. 10. The initial burst of convection in the

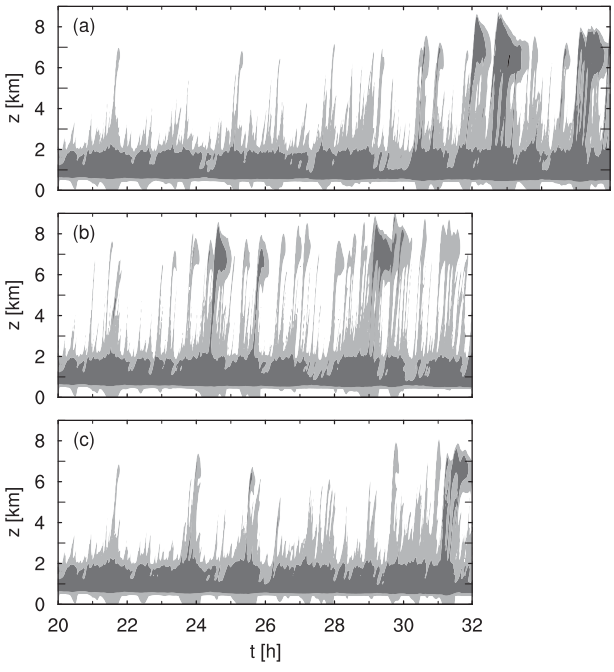

FIG. 7. Time series of $\overline{q}_l$ for (a) the control run and the simulations restarted at $t = 20$ h with no subgrid-scale mixing of (b) q_v and (c) θ. The control simulation is shown for $20 \leq t \leq 36$ h to facilitate comparison of the deep convection in the three simulations. Other details are as in Fig. 2.

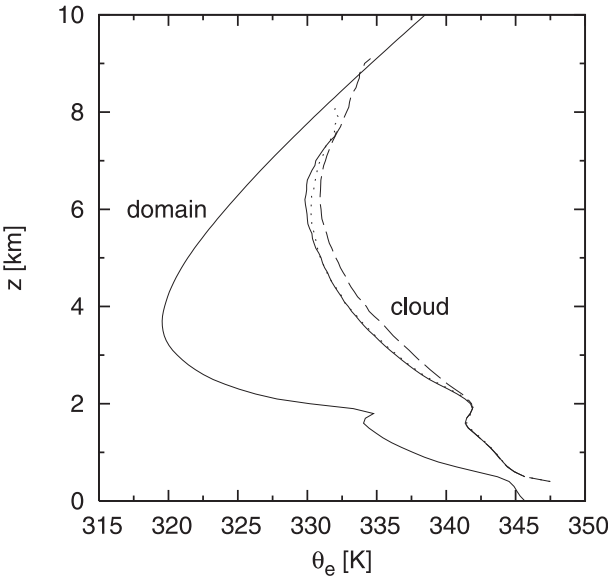

FIG. 8. Profiles of domain- and cloud-averaged θ_e in the control run (solid) and simulations restarted at $t = 20$ h with no subgrid-scale mixing of q_v (dashed) and θ (dotted; nearly indistinguishable from solid). Profiles are averaged in time over $20 \leq t \leq 32$ h.

spinup phase, which is seen in Fig. 9 to penetrate much higher than in the control run, is associated with the delayed onset of convection and increased buildup of CAPE. In the low-resolution simulation, the CAPE after this initial burst is lower than in the control run. Indeed, CAPE values just before the onset of the first deep clouds (near $t = 15$ h in the low-resolution simulation and $t = 30$ h in the control run) are smaller by a factor of 2 in the low-resolution simulation compared to the control run. Figure 11 shows instantaneous profiles of θ and q_v at $t = 15$ h in the low-resolution and control runs. The cloud layer between 1 and 2 km is marginally cooler and moister with low resolution, but the free-tropospheric profiles are essentially identical. These findings suggest that the accelerated transition to deep convection is not due to increased convective instability with coarse resolution.

The evolution of the 2D simulation is somewhat different. CAPE values are higher than in the control run over the first 30 h of integration, a discrepancy that appears to be due to an enhanced buildup of moisture in the mixed layer in the 2D simulation (not shown). Nevertheless, it is clear from Fig. 10 that (just as was true for the low-resolution experiment) the 2D simulation transitions to deep convection at a CAPE value that is significantly lower than that of the control run (approximately 1500 and 2000 $m^2\ s^{-2}$, respectfully). These tests indicate that the high-resolution 3D simulation is able to withstand higher values of CAPE without producing deep clouds than either the low-resolution or 2D runs.

d. *The role of free-tropospheric moistening and cooling*

As indicated by the profiles and time series of water vapor in Figs. 4 and 5, the transition from shallow to deep cumulus is associated with an increase in moisture in both the boundary layer and free troposphere. However, without further analysis, the causal relationship between moistening and deepening in these results is ambiguous. Figure 6 shows that the extension of moistening into the free troposphere is a consequence of congestus deepening but does not indicate whether this deepening is a consequence of moistening. Kuang and Bretherton (2006) addressed this question by restarting their simulation in the early congestus phase with a moist reference vapor sounding in the free troposphere taken from a later time, which was inside the deep convective regime. They observed that increased horizontally averaged humidity resulted in accelerated congestus deepening. Though extremely suggestive, this experiment is somewhat inconclusive because their moist profile was taken from a relatively late time in their control simulation, when deep convection was already present and moistening had already extended well above 4 km. To further

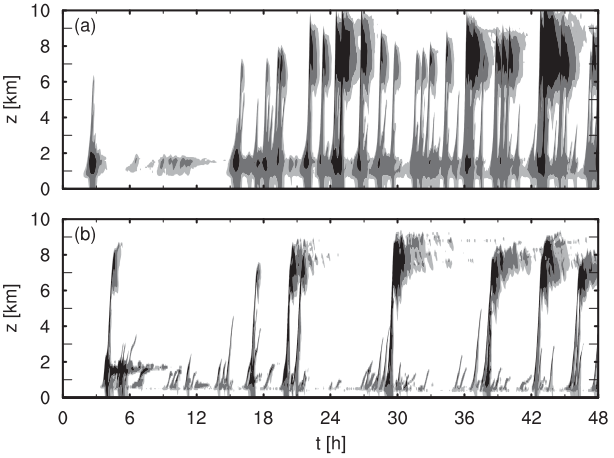

FIG. 9. Time series of $\overline{q}_l$ for the simulations with (a) $\Delta x = 500$ m and (b) only one horizontal spatial dimension. Other details are as in Fig. 2.

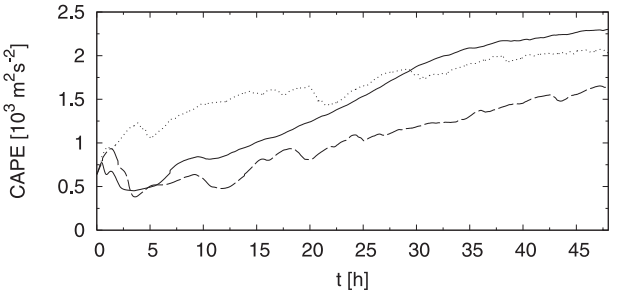

FIG. 10. Time series of CAPE from the control run (solid) and the simulations with $\Delta x = 500$ m (dashed) and only one horizontal dimension (dotted).

examine this question, we have performed additional sensitivity experiments in which the mean humidity profile was enhanced and extended the analysis further. A horizontally uniform perturbation is added to the vapor field for $z \geq 2$ km to yield a free-tropospheric moisture profile equal to that from a later reference time when the troposphere is moister. We use two reference times: $t = 32$ h, which corresponds to the start of the deep phase, and $t = 48$ h, which is well inside the deep convection regime (see Fig. 2b for a comparison of the two profiles). It should be noted that although the free-tropospheric humidity is increasing over the duration of the control simulation, these two reference profiles are still significantly drier than the moist profiles of Takemi et al. (2004) and Derbyshire et al. (2004). Simulations were restarted with the enhanced moisture profiles at $t =$ 20 h, which corresponds to the start of the transition phase, and run for 12 h to evaluate the implications for the transition to deep convection.

Time series of $\overline{q}_l$ are plotted in Fig. 12 for the control run (Fig. 12a) and both sensitivity experiments (Figs. 12b,c). It is apparent that enhancing the mean humidity profile results in a faster transition to the deep regime, and this effect is stronger for the $t = 48$ h profile, in which the moisture perturbation has a larger magnitude and extends further in the vertical. The implications for cloud entrainment can be evaluated from the cloud-averaged profiles of equivalent potential temperature (Fig. 13), which show that increasing the mean moisture results in less dilution of cloud θ_e in the free troposphere. By comparing Figs. 8 and 13, it is evident that increasing tropospheric moisture to the deep convection profile ($t = 48$ h) has a similar, though slightly weaker, effect on entrainment as omitting the subgrid-scale mixing of q_v.

While boosting the mean moisture of the free troposphere accelerates the transition to deep convection, this effect is not immediate. For the restart experiment with the $t = 32$ h reference profile, the development of deep clouds occurs only a few hours earlier than in the control run; before this time, the evolution of $\overline{q}_l$ in the restarted simulation is qualitatively similar to the control run. The $t = 48$ h vapor profile has a more significant effect, with deep clouds forming approximately 6 h earlier than in the control run but still 6 h after the enhanced humidity was introduced. Even though the $t = 48$ h profile is associated with deep clouds in the control run, the model nevertheless takes several hours to respond to the moisture and generate similarly deep clouds. Interestingly, the analogous experiment in Kuang and Bretherton (2006) also exhibits deep convection only around 6 h after the introduction of the moist sounding, despite the fact that

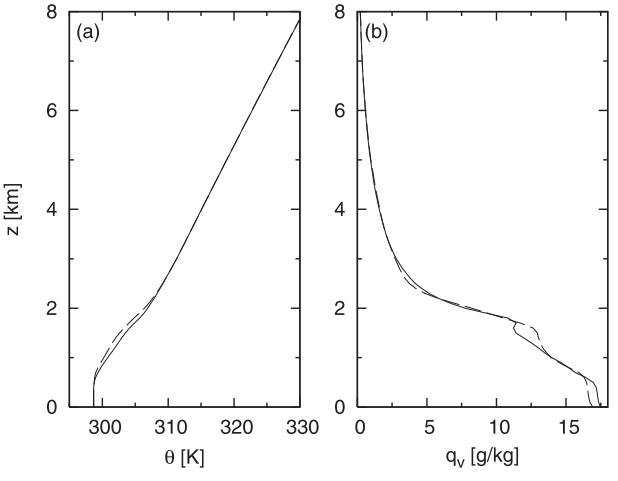

FIG. 11. Instantaneous horizontally averaged profiles of (a) θ and (b) q_v in the control run (solid) and the simulation with $\Delta x = 500$ m (dashed) at $t = 15$ h.

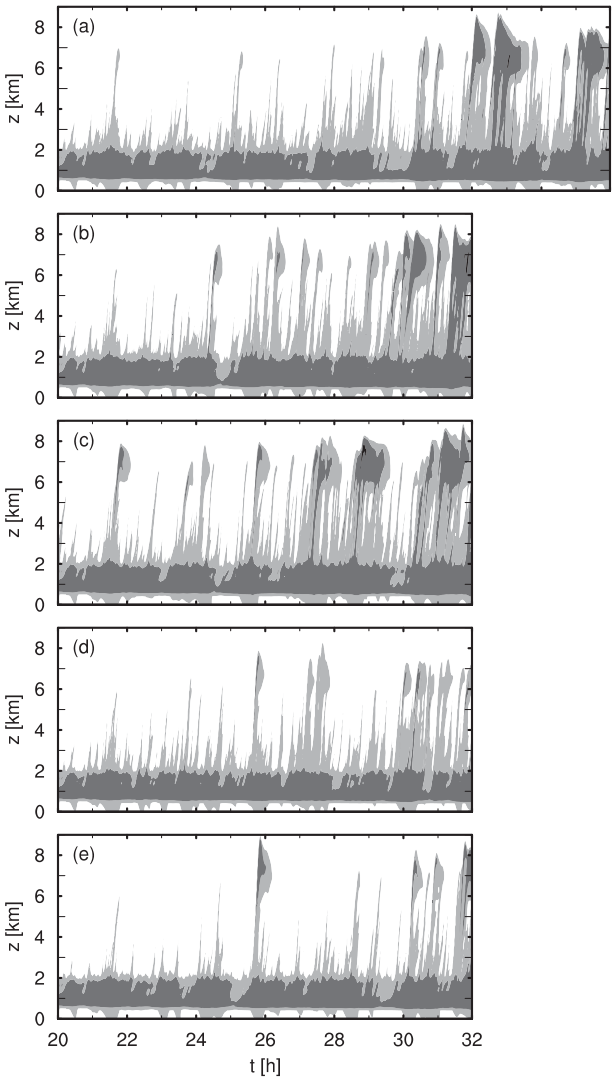

FIG. 12. Time series of $\overline{q}_l$ for (a) the control run, the simulations restarted at $t = 20$ h with mean free-tropospheric vapor profiles taken from (b) $t = 32$ h and (c) $t = 48$ h, and from the simulations restarted at $t = 20$ h with mean free-tropospheric potential temperature profiles taken from (d) $t = 32$ h and (e) $t = 48$ h. Other details are as in Fig. 2.

their reference profile is associated with deep convection in the control run. Figure 14a shows time series of CAPE in the moist sensitivity experiments, which closely follow that in the control run. A steady increase in CAPE is evident over the time interval. The observed delay in the onset of deep convection may therefore be due to the buildup of CAPE through the imposed cooling and surface fluxes. Even under more humid conditions, deep convection requires sufficient CAPE, which is not present in our control run at $t = 20$ h. However, the CAPE required for deep convection decreases significantly as the

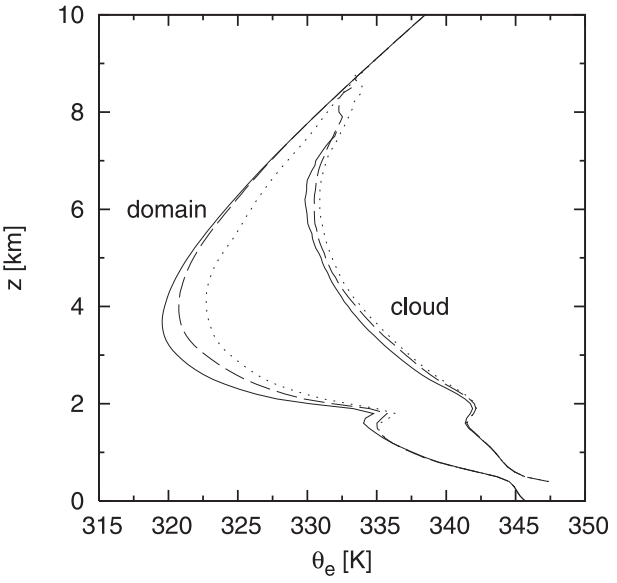

FIG. 13. Profiles of domain- and cloud-averaged θ_e in the control run (solid) and simulations restarted at $t = 20$ h with mean free-tropospheric vapor profiles taken from $t = 32$ h (dashed) and $t = 48$ h (dotted). Profiles are averaged in time over $20 \leq t \leq 32$ h.

magnitude and vertical extent of the free-tropospheric moisture increases.

In addition to moistening, the free troposphere cools over the course of the control run (Figs. 2c and 4c), and it is instructive to also assess the role of this cooling on the transition to deep convection. To address this question, we have performed two additional sensitivity

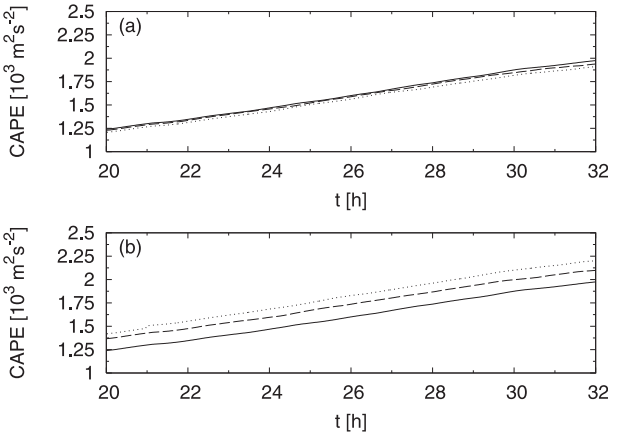

FIG. 14. Time series of CAPE from (a) moist restart experiments with q_v profiles from $t = 32$ h (dashed) and 48 h (dotted) and (b) the cool restart experiments with θ profiles from $t = 32$ h (dashed) and 48 h (dotted). The control run CAPE (solid) is also plotted in both panels. As expected, CAPE values from the moist restart experiments lie slightly below the control run, while the cool restart experiments have higher CAPE values.

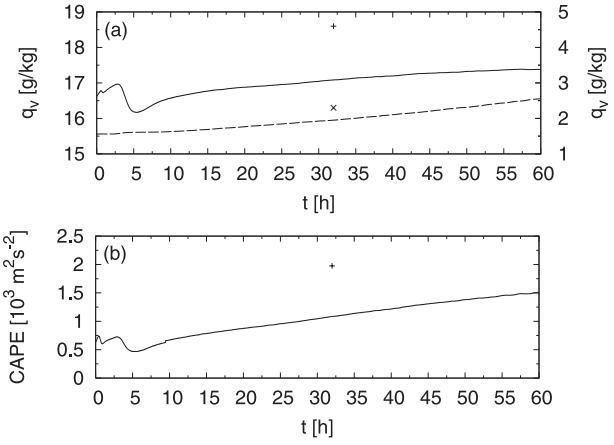

FIG. 15. (a) Time series of mixed layer q_v (solid; left y axis) and lower free troposphere q_v (dashed; right y axis) from the simulation with mixed layer drying. (b) Time series of CAPE from the same simulation. Values from the control run at $t = 32$ h, corresponding to the onset of deep convection in that simulation, are included for comparison (plus sign for mixed-layer q_v and CAPE; ex for free-tropospheric q_v). Other details are as in Fig. 5.

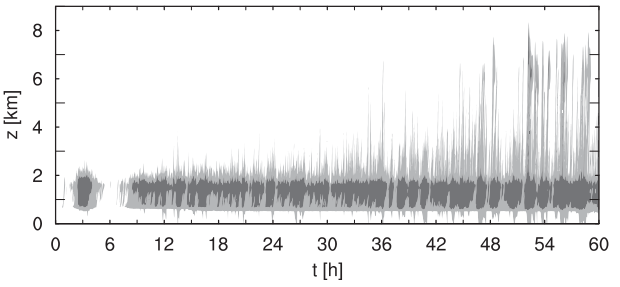

FIG. 16. Time series of $\overline{q}_l$ from the simulation with mixed layer drying. Other details are as in Fig. 2.

experiments, in which a horizontally uniform negative potential temperature perturbation was added at $t = 20$ h to yield a cooler free-tropospheric sounding equal to that from a later time in the control run. As for the moist sensitivity tests described above, the perturbation was applied for $z \geq 2$ km, and two reference times were employed: $t = 32$ and 48 h. The resulting time series of $\overline{q}_l$ are shown in Figs. 12d,e. The effect on cloud depth is significantly weaker than that of the moisture perturbations, even though the CAPE in the cool simulations is significantly higher than that in the control and moist sensitivity tests (Fig. 14b).

e. The role of boundary layer moisture

The cloud deepening of the control simulation is associated with moistening in the boundary layer as well as the free troposphere, as indicated by the bulk vapor time series in Fig. 5. The rise in boundary layer θ_e and the free tropospheric cooling are the two main mechanisms that contribute to the increase in CAPE. To evaluate the separate effect of boundary layer moisture on cloud depth, we have performed an additional simulation with a prescribed drying term to reduce the moistening at low levels. This forcing imposes a uniform drying rate in the q_v equation of 5 g kg^{-1} day^{-1} for $0 \leq z \leq 300$ m, decreasing linearly to zero at $z = 500$ m, following Siebesma et al. (2003), who included a term with similar structure but smaller magnitude. Time series of vertically averaged mixed layer and free-tropospheric water vapor are plotted in Fig. 15. The mixed layer in this simulation is much drier than in the control run, with average humidity less than 17.5 g kg^{-1} for $0 \leq t \leq 60$ h, compared to values as high as 19 g kg^{-1} at the end of the control run.

The evolution of $\overline{q}_l$ is shown in Fig. 16. As in the control run, shallow cumulus form at an early stage in the simulation, and after several hours they start to gradually grow in height. Deep clouds, with tops above 8 km, appear around $t = 52$ h, 20 h later than in the control run. The average mixed layer moisture at the onset of deep convection is very different in these two simulations, with values of 18.6 g kg^{-1} in the control run at $t = 32$ h and 17.3 g kg^{-1} in the dry mixed layer simulation at $t = 52$ h; the difference in CAPE is correspondingly significant (cf. Figs. 5 and 15). However, there is remarkable agreement in the free-tropospheric moisture at the onset of deep convection: vertically averaged water vapor over $2 \leq z \leq 5$ km is 2.3 g kg^{-1} in the control run at $t = 32$ h and 2.4 g kg^{-1} in the dry mixed layer run at $t = 52$ h. The close relationship between cloud height and free-tropospheric moisture therefore persists in the presence of very different forcings.

4. Summary and discussion

High-resolution cloud-resolving simulations were employed to investigate and assess the transition of cumulus clouds from shallow to congestus to deep convection. An idealized approach was followed, in which simulations were initialized with soundings representative of a shallow cumulus regime and forced with specified horizontally uniform SSTs and radiative cooling. The transition to deep convection was achieved by ignoring the large-scale subsidence and advective forcings that sustained trade wind cumulus in the BOMEX observations from which the initial conditions were derived (Siebesma et al. 2003). Over the course of two days, the control simulation passes through three phases: a shallow cumulus regime, which persists for approximately 16 h; a transition phase characterized by deepening

congestus clouds, which lasts for approximately 12 h; and a deep convection regime. This transition from shallow to deep convection is faster than that obtained by Kuang and Bretherton (2006), who initiated deepening by increasing the surface fluxes in the presence of large-scale forcings. Deep convective clouds in our simulations are limited to depths of less than 10 km, likely because of the static stability of the upper troposphere, although the simplified microphysics (which neglect latent heating from freezing; see Grabowski 1998) may also play a role.

The fact that moister environments favor deeper convection has been established in previous simulations of statistically stationary convective regimes (Derbyshire et al. 2004; Takemi et al. 2004), and this coupling is manifested in our simulations, in which both quantities are found to increase in time. However, here we have addressed the important question of how and why this coupling occurs by identifying the various physical mechanisms responsible and quantifying them through changes to simulation parameters and configurations. The connection between moisture and cloud depth can work in two directions: clouds can modify the moisture of their environment, and moister environments may promote deeper clouds. The first effect is clearly apparent in our simulations, in which congestus clouds were found to moisten the lower troposphere at a rate of approximately 2 g kg^{-1} day^{-1}. This moistening results from resolved advective flux convergence over levels occupied by clouds; the horizontally averaged contributions of subgrid-scale vapor mixing and evaporation are an order of magnitude smaller. As the congestus clouds deepen, the moistening extends further into the troposphere. For larger-scale flows such as synoptic-scale convectively coupled waves, this cloud-driven moistening will be augmented by organized horizontal moisture convergence (e.g., Johnson et al. 1999; Khouider and Majda 2006; Takayabu et al. 2010).

The second part of the relationship between environmental moisture and cloud depth—the tendency of increased tropospheric humidity to precondition the environment for deep convection—is more challenging to diagnose. The proposed explanation for this effect is dry-air entrainment (e.g., Brown and Zhang 1997; Holloway and Neelin 2009), and we have confirmed the importance of this mechanism in limiting the cloud heights in a number of sensitivity tests. Eliminating subgrid-scale mixing of water vapor in our simulations reduces the dilution of cloudy air, which enhances latent heating and allows the clouds to attain greater heights. By contrast, eliminating subgrid-scale mixing of potential temperature had no significant impact on cloud depth. Similarly, changes to simulation parameters that result in reduced resolved mixing of environmental air into the clouds—e.g. lower horizontal resolution or restricting to one horizontal dimension—were found to significantly accelerate the transition from shallow to deep convection.

As the lower troposphere moistens, the impact of entrainment on cloud buoyancy is reduced because the environmental air mixed into clouds is less dry. This tendency may account for the transition to deep convection in our simulations, and we have evaluated this hypothesis with two sensitivity tests, in which horizontally uniform moisture perturbations were introduced in the early congestus phase. The perturbations were chosen to yield a mean free-tropospheric moisture profile equal to that from a later reference time. Two reference times were considered: one corresponding to the start of the deep convective phase and the other taken from after the appearance of deep convection (as in Kuang and Bretherton 2006). We found that enhanced free-tropospheric moisture does indeed lead to reduced cloud dilution and an accelerated transition to deeper clouds. However, the cloud field does not respond instantaneously to the enhanced moisture profile but rather takes several hours to adjust, likely because of the buildup of CAPE. Nevertheless, this delay decreases as the free-tropospheric moisture is increased, suggesting that less CAPE is required for deep convection in moister environments. For the moister reference profile, this delay is approximately 6 h. A similar delay is apparent in the results of Kuang and Bretherton (2006), though it was not discussed.

We performed other sensitivity tests to examine the separate dependence of deep convection on free-tropospheric temperature and boundary layer moisture, both of which contribute to CAPE. These included restart experiments in which the potential temperature field was modified to correspond to the cooler free-tropospheric conditions of the deep convective phase. Despite the increase in CAPE associated with these perturbations, the transition to deep convection was not significantly accelerated. We also performed a separate experiment in which the boundary layer moisture was reduced through a drying term, suppressing the buildup of CAPE. The eventual transition to deep convection was found to occur only when the midtropospheric moisture was comparable to that of the control run. These tests indicate that the transition to deep convection in our simulation is determined primarily by the moistening of the free troposphere; the cooling of the troposphere and moistening of the boundary layer are of secondary importance.

The effect of turbulent mixing of dry air into rising plumes is identified here as the main mechanism that inhibits deep convection when the free troposphere is

dry. However, this important process presents a challenge for atmospheric simulations with both parameterized and explicit convection. Our results show that even for cloud-resolving simulations, the depth of simulated clouds may be strongly sensitive to subgrid-scale turbulence parameterizations, grid resolution, and dimensionality. Indeed, we were able to accelerate the transition phase of the simulation, during which congestus clouds gradually build into deep convection over $O(10)$ h, by increasing the grid scale to $\Delta x = 500$ m or by neglecting the dependence on one horizontal dimension. Cloud-resolving simulations with two dimensions and grid scales $O(1)$ km are widely employed, especially when large domains are necessary. The significance of the sensitivity of cloud depth on these parameters and the implications for the accurate representation of congestus preconditioning in simulations of convectively coupled waves clearly deserve further study.

The conclusions of this work may be used to improve model parameterizations for organized tropical convection. We have quantified several key physical processes in the transition from shallow to deep convection by moisture preconditioning. These findings include a 2 g kg day^{-1} moistening rate due to the detrainment of congestus clouds, a congestus cloud lifetime of approximately 20 min, and a moist layer extending up to 6 km during the deep convection regime. Such results can be exploited and directly incorporated into convective parameterizations such as the multicloud stochastic model of Khouider et al. (2010).

Acknowledgments. We thank the anonymous referees for helpful comments on the manuscript. This work was supported by a Pacific Institute for the Mathematical Sciences postdoctoral fellowship (MLW), as part of the Collaborative Research Group on Mathematical Problems in Climate Modelling, and grants from the Canadian Foundation for Climate and Atmospheric Sciences and the Natural Sciences and Engineering Research Council of Canada (BK). The authors are grateful to Wojciech Grabowski and Piotr Smolarkiewicz for providing the numerical code and assistance with the setup of the simulations.

REFERENCES

Brown, R. G., and C. Zhang, 1997: Variability of midtropospheric moisture and its effect on cloud-top height distribution during TOGA COARE. *J. Atmos. Sci.,* **54,** 2760–2774.

Derbyshire, S. H., I. Beau, P. Bechtold, J.-Y. Grandpeix, J.-M. Piriou, J.-L. Redelsperger, and P. M. M. Soares, 2004: Sensitivity of moist convection to environmental humidity. *Quart. J. Roy. Meteor. Soc.,* **130,** 3055–3079.

Grabowski, W. W., 1998: Towards cloud-resolving modeling of large-scale tropical circulations: A simple cloud microphysics parameterization. *J. Atmos. Sci.,* **55,** 3283–3298.

——, and P. K. Smolarkiewicz, 1990: Monotone finite-difference approximations to the advection–condensation problem. *Mon. Wea. Rev.,* **118,** 2082–2098.

——, and ——, 2002: A multiscale anelastic model for meteorological research. *Mon. Wea. Rev.,* **130,** 939–956.

Haertl, P. T., and G. N. Kiladis, 2004: Dynamics of 2-day equatorial disturbances. *J. Atmos. Sci.,* **61,** 2707–2721.

Holloway, C. H., and J. D. Neelin, 2009: Moisture vertical structure, column water vapor, and tropical deep convection. *J. Atmos. Sci.,* **66,** 1665–1683.

Johnson, R. H., T. M. Rickenbach, S. A. Rutledge, P. E. Ciesielski, and W. H. Schubert, 1999: Trimodal characteristics of tropical convection. *J. Climate,* **12,** 2397–2418.

Khouider, B., and A. J. Majda, 2006: A simple multicloud parameterization for convectively coupled tropical waves. Part I: Linear analysis. *J. Atmos. Sci.,* **63,** 1308–1323.

——, and ——, 2008: Multicloud models for organized tropical convection: Enhanced congestus heating. *J. Atmos. Sci.,* **65,** 895–914.

——, J. Biello, and A. J. Majda, 2010: A stochastic multicloud model for tropical convection. *Commun. Math. Sci.,* **8,** 187–216.

Kiladis, G. N., K. H. Straub, and P. T. Haertel, 2005: Zonal and vertical structure of the Madden–Julian oscillation. *J. Atmos. Sci.,* **62,** 2790–2809.

——, M. C. Wheeler, P. T. Haertel, K. H. Straub, and P. E. Roundy, 2009: Convectively coupled equatorial waves. *Rev. Geophys.,* **47,** RG2003, doi:10.1029/2008RG000266.

Kuang, Z., and C. S. Bretherton, 2006: A mass-flux scheme view of a high-resolution simulation of a transition from shallow to deep cumulus convection. *J. Atmos. Sci.,* **63,** 1895–1909.

Lilly, D. K., 1962: On the numerical simulation of buoyant convection. *Tellus,* **14,** 148–172.

Lin, J. L., and Coauthors, 2006: Tropical intraseasonal variability in 14 IPCC AR4 climate models. Part I: Convective signals. *J. Climate,* **19,** 2665–2690.

Nitta, T., and S. Esbensen, 1974: Heat and moisture budget analyses using BOMEX data. *Mon. Wea. Rev.,* **102,** 17–28.

Siebesma, A. P., and Coauthors, 2003: A large-eddy simulation intercomparison study of shallow cumulus convection. *J. Atmos. Sci.,* **60,** 1201–1219.

Smagorinsky, J., 1963: General circulation experiments with the primitive equations. I. The basic experiment. *Mon. Wea. Rev.,* **91,** 99–164.

Smolarkiewicz, P. K., and L. G. Margolin, 1998: MPDATA: A finite-difference solver for geophysical flows. *J. Comput. Phys.,* **140,** 459–480.

——, and J. M. Prusa, 2005: Towards mesh adaptivity for geophysical turbulence: Continuous mapping approach. *Int. J. Numer. Methods Fluids,* **47,** 789–801.

Straub, K. H., and G. N. Kiladis, 2002: Observations of a convectively coupled Kelvin wave in the eastern Pacific ITCZ. *J. Atmos. Sci.,* **59,** 30–53.

Takayabu, Y. N., S. Shige, W.-K. Tao, and N. Hirota, 2010: Shallow and deep latent heating modes over tropical oceans observed with TRMM PR spectral latent heating data. *J. Climate,* **23,** 2030–2046.

Takemi, T., O. Hirayama, and C. Liu, 2004: Factors responsible for the vertical development of tropical oceanic cumulus convection. *Geophys. Res. Lett.,* **31,** L11109, doi:10.1029/2004GL020225.

Tulich, S. N., D. A. Randall, and B. E. Mapes, 2007: Vertical-mode and cloud decomposition of large-scale convectively coupled gravity waves in a two-dimensional cloud-resolving model. *J. Atmos. Sci.,* **64,** 1210–1229.

Waite, M. L., and B. Khouider, 2009: Boundary layer dynamics in a simple model for convectively coupled gravity waves. *J. Atmos. Sci.,* **66,** 2780–2795.

Yanai, M., S. Esbensen, and J.-H. Chu, 1973: Determination of bulk properties of tropical cloud clusters from large-scale heat and moisture budgets. *J. Atmos. Sci.,* **30,** 611–627.

Zhang, C., and M.-D. Chou, 1999: Variability of water vapor, infrared radiative cooling, and atmospheric instability for deep convection in the equatorial western Pacific. *J. Atmos. Sci.,* **56,** 711–723.

——, and S. M. Hagos, 2009: Bi-modal structure and variability of large-scale diabatic heating in the tropics. *J. Atmos. Sci.,* **66,** 3621–3640.

Zhao, M., and P. H. Austin, 2005: Life cycle of numerically simulated shallow cumulus clouds. Part I: Transport. *J. Atmos. Sci.,* **62,** 1269–1290.